Supporting information

Interlayer ionic diffusion driven in situ QDs-deposition in Co_9S_8-LDH hybrid supercapacitor electrode

Yanan Zhang[a]*, Nuo Xu[a], Jipeng Xu[a], Chi Shan[a], Junlei Chen[a], Liyuan Guo[a], Long Qin[bc], Fan Wu[c]* and Wenhuan Huang[a]*

[a] Key Laboratory of Chemical Additives for China National Light Industry, College of Chemistry and Chemical Engineering, Shaanxi University of Science and Technology, Xi'an, 710021, China

b School of Mechanical Engineering, Nanjing University of Science &Technology, Nanjing, 210094, China.

c Department of Chemistry, School of Science, Tianjin University, Tianjin, 300072, China.

Corresponding authors: zhangyanan@sust.edu.cn; wufan0817@tju.edu.cn; huangwenhuan@sust.edu.cn.

Contents

1. EXPERIMENTAL SECTION

1.1. Materials

Cobalt nitrate hexahydrate ($Co(NO_3)_2 \cdot 6H_2O$), nickel nitrate hexahydrate ($Ni(NO_3)_2 \cdot 6H_2O$), potassium hydroxide (KOH) and poly(1,1-difluoroethlene) (PVDF) were purchased from Aladdin Chemical Reagent Co., Ltd. Trimesic acid (H_3BTC), ethanol, N,N-dimethylformamide (DMF), carbon cloth (WOS1009) and activeted carbon (AC)were provided by Sinopharm Chemical Reagent Co., Ltd.

1.2. Material characterization

The morphological structure was obtained by scanning electron microscope (SEM, Verios 460). The microstructure of the samples was observed using a transmission electron microscope (HITACHI HT-7700) with an accelerating voltage of 100 kV. The High-resolution transmission electron microscopy (HRTEM) images were acquired using Titan G260-300 microscopy (FEI, USA). The crystal phase was performed by X-ray diffraction (XRD) on a Bruker D8 Advanced X-ray Diffractometer with Cu-Kα radiation (λ = 1.54056 Å). The X-ray photoelectron spectroscopy measurement (XPS, ESCALab250, USA) was recorded to analyze the surface chemical composition and states of the samples with monochromatic 150 W Al-K(α) radiation.

1.3 Electrochemical measurements of single electrodes

The electrochemical performance was measured at ambient temperature in the standard three-electrode system with an electrochemical workstation (CHI660E). Specially, the prepared materials were acted as the working electrodes, while a platinum wire, a saturated Hg/HgO electrode and 6 M KOH solution were used as the counter electrode, reference electrode and electrolyte, respectively. The electrochemical performance of electrodes was measured by cyclic voltammetry (CV), galvanostatic charge discharge (GCD), and electrochemical impedance spectroscopy (EIS).

The mass specific capacitance and specific capacity was calculated according to the following equations, respectively[1].

$$C_m = \frac{I \times \Delta t}{m \times \Delta V}$$

$$Qs = \frac{I\,\Delta t}{3.6\,m}$$

where C_m, I, Δt, ΔV, m and Q_s are the gravimetric specific capacitance (F g^{-1}), discharge current (A), discharge time (s), voltage window (V), the mass of active materials (g), and specific capacity (mAh g^{-1}), respectively.

1.4 Electrochemical measurements of HSCs

The test of the two electrodes is also examined in 6 M KOH solution. QDs-Co_9S_8/CoNi-LDH and AC are used as positive and negative electrode materials. The preparation method of the negative electrode material is activated carbon, PVDF and carbon black by mixing and grinding with a mass ratio of 8:1:1, using NMP as wetting agent. Finally, the ink is coated on the carbon cloth and the load is about 1.5 mg cm^{-2}. Before measuring the QDs-Co_9S_8/CoNi-LDH//AC capacitor, the mass ratio between the positive electrode and the negative electrode is calculated by the balance charge formula:

$$M_+/M_- = (C_-\triangle V_-)/(C_+\triangle V_+)$$

The energy density (Wh kg^{-1}) and power density (W kg^{-1}) was calculated according to the following equations, respectively.

$$E = \frac{C \times \Delta V^2}{7.2}$$

$$P = \frac{3600\,E}{\Delta t}$$

1.5 Theoretical Calculations:

The density functional theory (DFT) calculations were carried out with the VASP code. The Perdew–Burke–Ernzerhof (PBE) functional within generalized gradient approximation (GGA) was used to process the exchange–correlation, while the projectoraugmented-wave pseudopotential (PAW) was applied with a kinetic energy cut-off of 500 eV, which was utilized to describe the expansion of the electronic eigenfunctions. The Brillouin-zone integration was sampled by a Γ-centered 10 × 10 × 1 Monkhorst–Pack k-point. All atomic positions were fully relaxed until energy and force reached a tolerance of 1 × 10^{-5} eV and 0.03 eV/Å, respectively. The dispersion corrected DFT-D method was employed to consider the long-range interactions.

2. RESULTS AND DISCUSSIONS

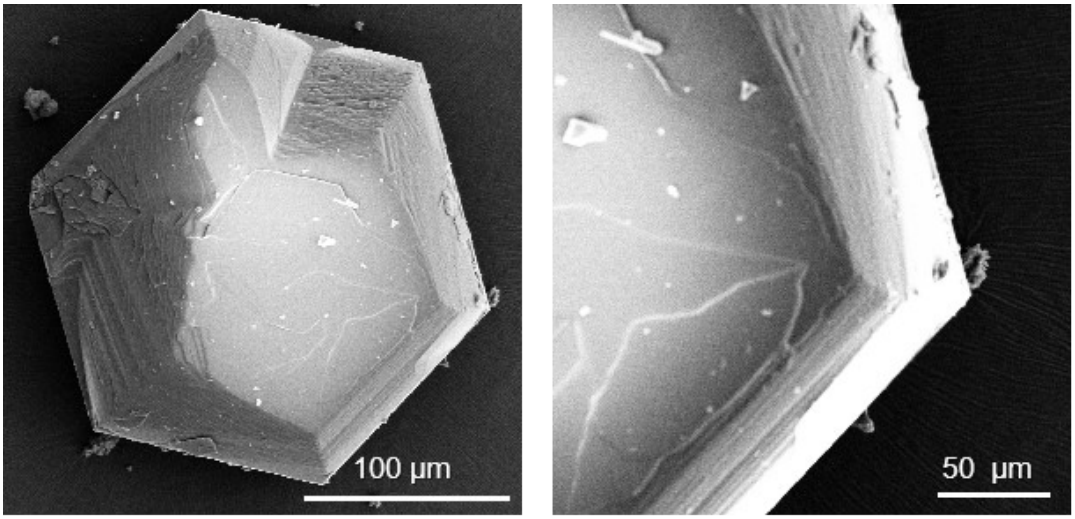

Figure S1.SEM images of Ni-BTC

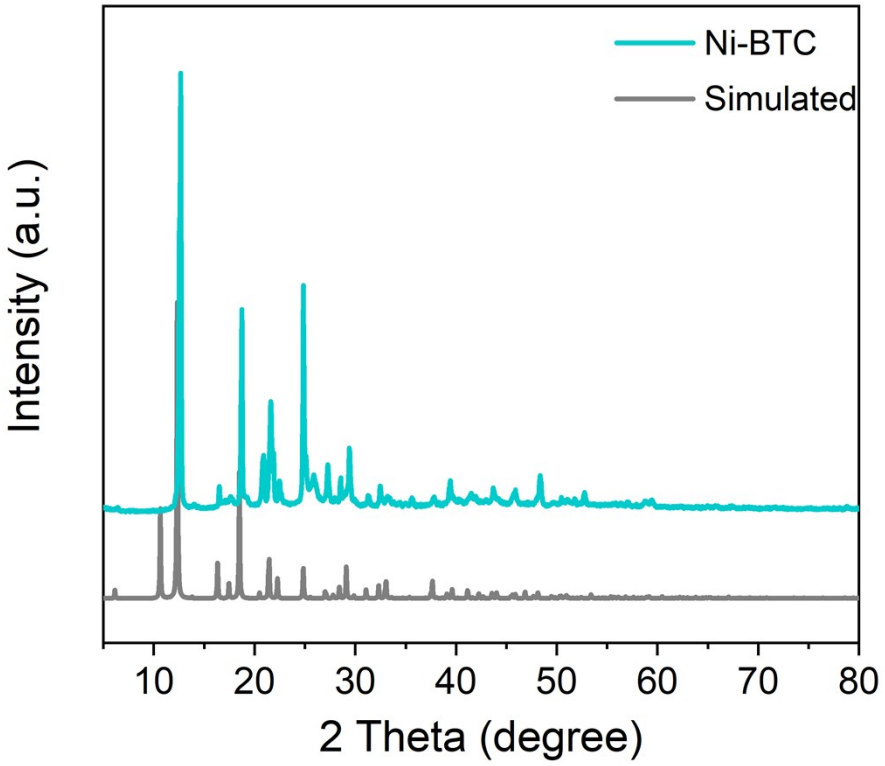

Figure S2. Experimental and simulated XRD patterns of Ni-BTC.

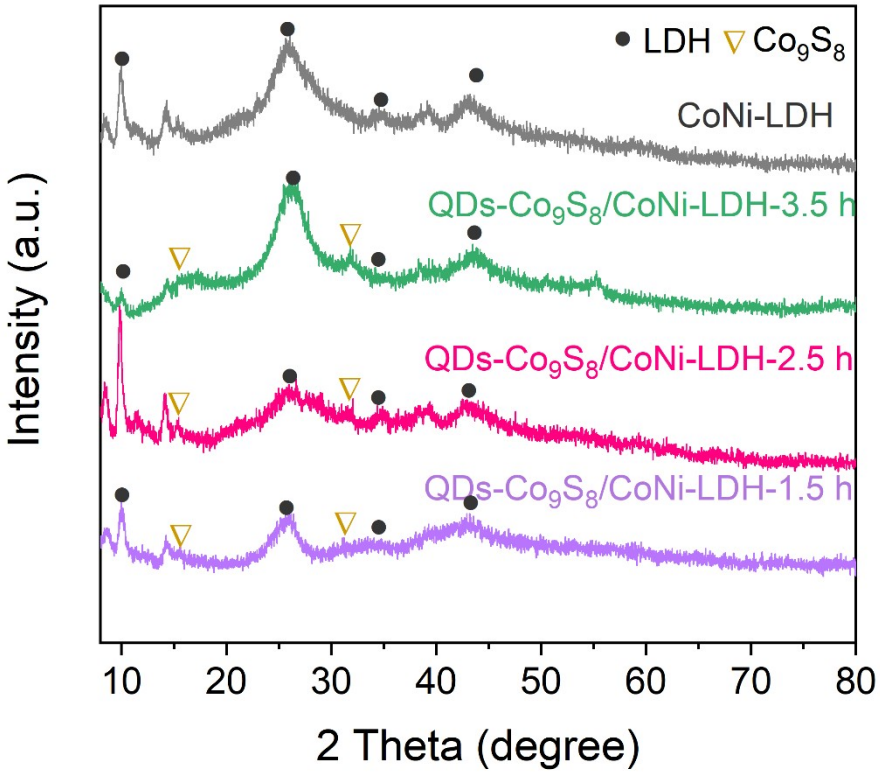

Figure S3. CoNi-LDH, QDs-Co_9S_8/CoNi-LDH XRD diffraction patterns at different time.

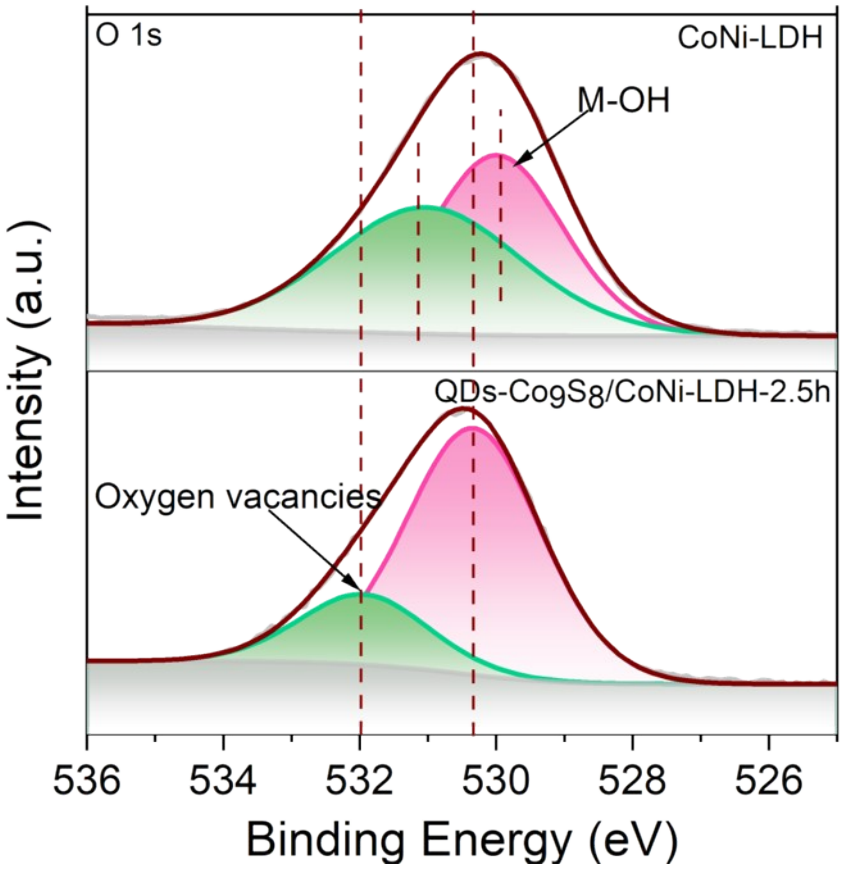

Figure S4. XPS spectra of O 1s for CoNi-LDH and QDs-Co9S8/CoNi-LDH-2.5 h

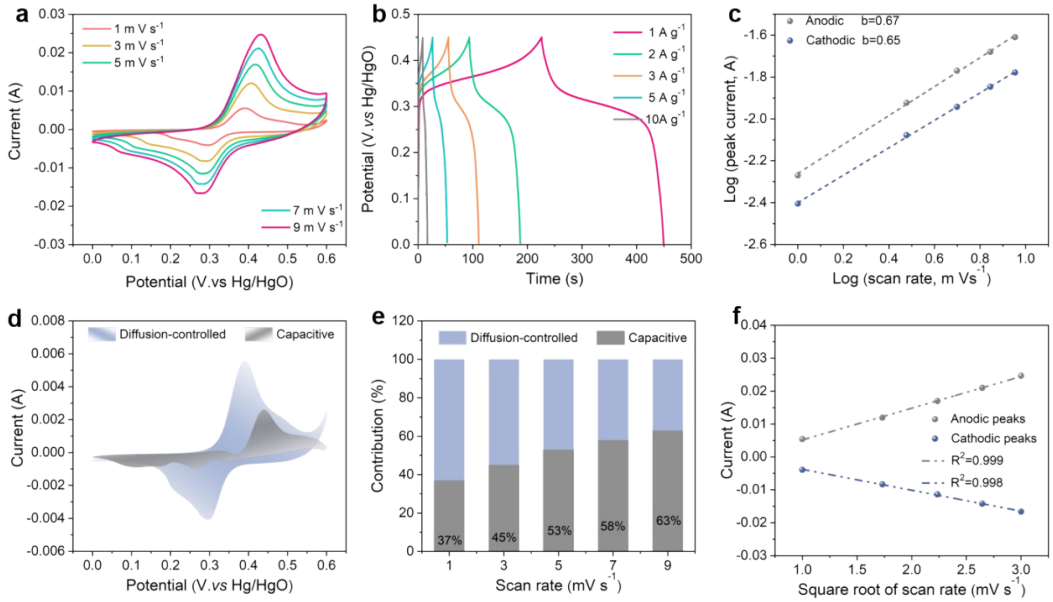

Figure S5. (a) CV curves , (b) GCD curves and (c) The plot of log (i) versus log (v) of CoNi-LDH; (d) Separation of the diffusion and capacitive-controlled currents for CoNi-LDH at a scan rate of 1 mV s^{-1}; (e) The diffusion and capacitance-controlled contribution for CoNi-LDH electrodes at different scan rates of 1, 3, 5, 7, 9 mV s^{-1};(f) Plots of anodic and corresponding cathodic peak versus the square root of scan rates for CoNi-LDH.

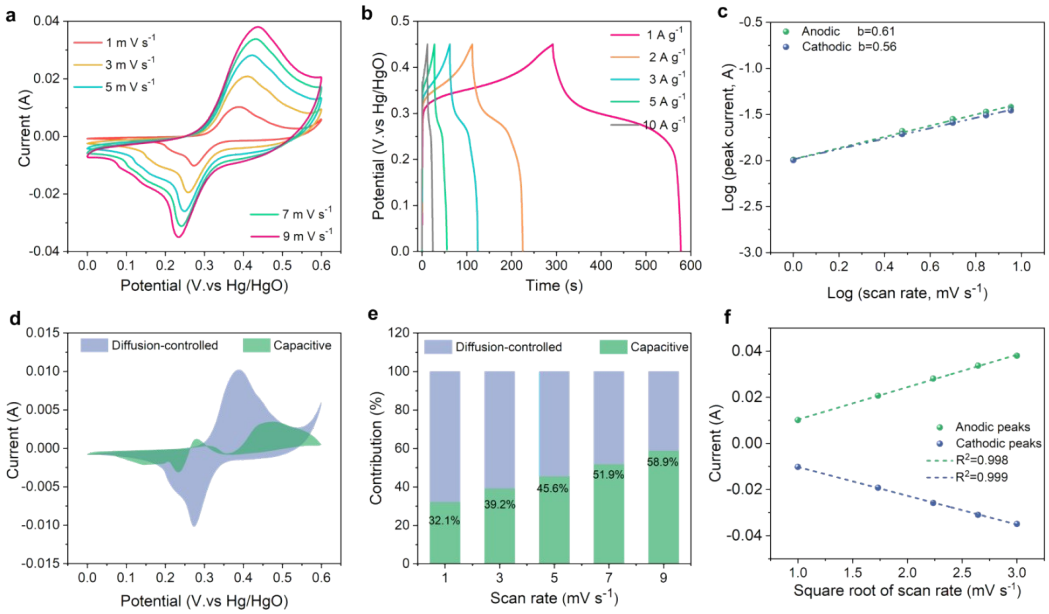

Figure S6. (a) CV curves, (b) GCD curves and (c) The plot of log (i) versus log (v) of QDs-Co_9S_8/CoNi-LDH-1.5 h; (d) Separation of the diffusion and capacitive-controlled currents for QDs-Co_9S_8/CoNi-LDH-1.5 h at a scan rate of 1 mV s^{-1}; (e) The diffusion and capacitance-controlled contribution for QDs-Co_9S_8/CoNi-LDH-1.5 h electrodes at different scan rates of 1, 3, 5, 7, 9 mV s^{-1};(f) Plots of anodic and corresponding cathodic peak versus the square root of scan rates for QDs-Co_9S_8/CoNi-LDH-1.5 h.

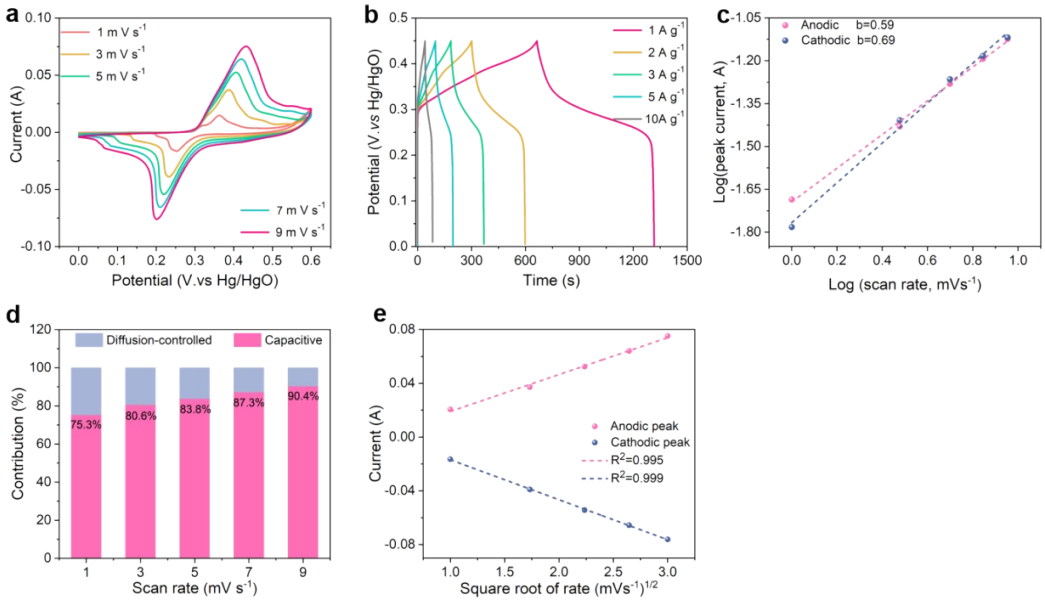

Figure S7. (a) CV curves, (b) GCD curves and (c) The plot of log (i) versus log (v) of QDs-Co_9S_8/CoNi-LDH-2.5 h; (d) The diffusion and capacitance-controlled contribution for QDs-Co_9S_8/CoNi-LDH-2.5 h electrodes at different scan rates of 1, 3, 5, 7, 9 mV s^{-1}; (e) Plots of anodic and corresponding cathodic peak versus the square root of scan rates for QDs-Co_9S_8/CoNi-LDH-2.5 h.

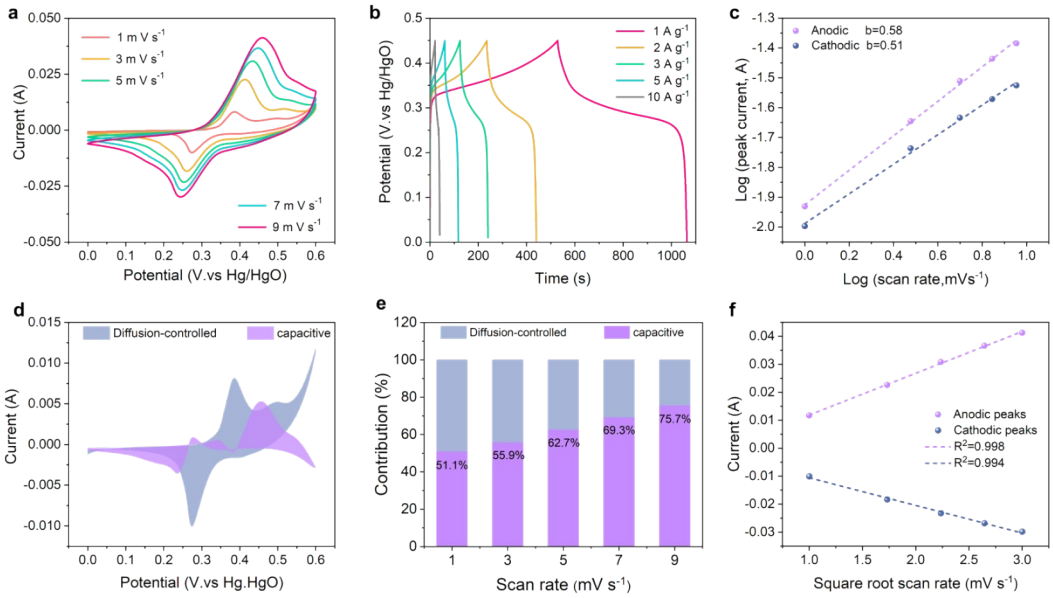

Figure S8. (a) CV curves , (b) GCD curves and (c) The plot of log (i) versus log (v) of QDs-Co_9S_8/CoNi-LDH-3.5 h; (d) Separation of the diffusion and capacitive-controlled currents for QDs-Co_9S_8/CoNi-LDH-3.5 h at a scan rate of 1 mV s^{-1}; (e) The diffusion and capacitance-controlled contribution for QDs-Co_9S_8/CoNi-LDH-3.5 h electrodes at different scan rates of 1, 3, 5, 7, 9 mV s^{-1};(f) Plots of anodic and corresponding cathodic peak versus the square root of scan rates for QDs-Co_9S_8/CoNi-LDH-3.5 h.

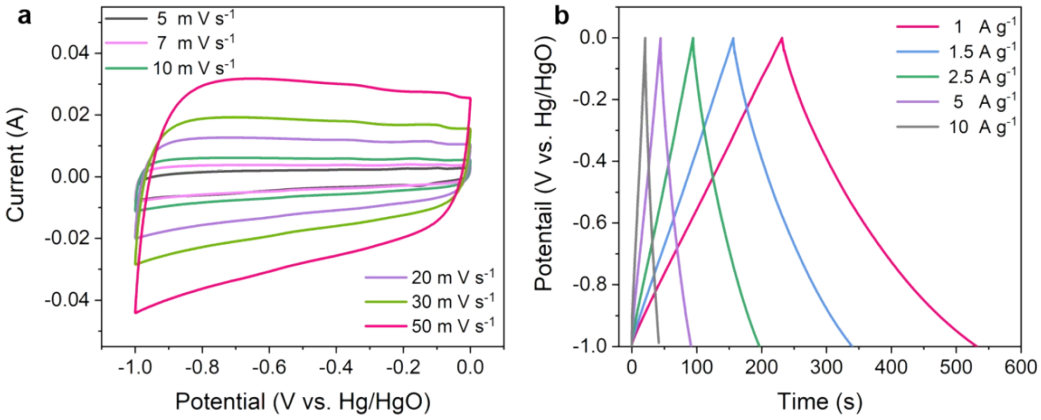

Figure S9. Electrochemical performance of AC: (a) CV curves at different scan rates, (b) GCD curves at various current densities of 1-10 A g^{-1}

Table S1. Comparison of supercapacitor performance of QDs-Co_9S_8/CoNi-LDH HSC with other MOFs derived double hydroxide materials.

Electrode Samples	Cs (*j*) $Fg^{-1}(1Ag^{-1})$	Energy density (Wh kg^{-1})	Power density (W kg^{-1})	Ref.
QDs-Co_9S_8/CoNi-LDH//AC	93.7(1)	33.3	820	This work
Co_9S_8/CNF-3//ACNFs	82.0 (0.5 A g^{-1})	23.8	750	[2]
Co_9S_8@$NiCo_2S_4$@NF// AC	95(1)	30	731.8	[3]
R-Co_3O_4/CoS//AC	85(1)	23.6	250	[4]
NiS@CoS//AC	75.9(1)	24.1	752.15	[5]
NiCo-LDH@$Ni(OH)_2$//AC	86.0(1)	30.6	799.9	[6]
CoNi-LDH//AC	57.3(1)	20.38	800.0	[7]
N-ZnCo-LDH//AC	93.5(1)	29.2	750.0	[8]

3. REFERENCES

[1] X. Gao, Y. Zhao, K. Dai, J. Wang, B. Zhang and X. Shen, NiCoP nanowire@NiCo-layered double hydroxides nanosheet heterostructure for flexible asymmetric supercapacitors, *Chemical Engineering Journal*, 2020, **384**, 12337.

[2] N. Zhang, W. Wang, C. Teng, Z. Wu, Z. Ye, M. Zhi and Z. Hong, Co_9S_8 nanoparticle-decorated carbon nanofibers as high-performance supercapacitor electrodes, *RSC Advances*, 2018, **8**, 27574-27579.

[3] Y. Yang, D. Qian, H. Zhu, Q. Zhou, Z. Zhang, Z. Li and Z. Hu, Construction of tremella-like Co_9S_8@$NiCo_2S_4$ heterostructure nanosheets integrated electrode for high-performance hybrid supercapacitorsConceptualization, Methodology, Formal analysis, *Journal of Alloys and Compounds*, 2022, **898**, 162850

[4] Y. Lu, W. Yang, W. Li, M. Chen, L. Shuai, P. Qi, D. Zhang, H. Du, Y. Tang and M. Qiu, Room-temperature sulfurization for obtaining Co_3O_4/CoS core-shell nanosheets as supercapacitor electrodes, *Journal of Alloys and Compounds*, 2020, **818**, 152877.

[5] Y. Miao, X. Zhang, J. Zhan, Y. Sui, J. Qi, F. Wei, Q. Meng, Y. He, Y. Ren, Z. Zhan and Z. Sun, Hierarchical NiS@CoS with Controllable Core-Shell Structure by Two-Step Strategy for Supercapacitor Electrodes, *Advanced Materials Interfaces*, 2019, **7**, 1901618.

[6] W. Cao, W. Zhao, C. Xiong, Q. Long, N. Chen and G. Du, NiCo-MOF derived nanostructured NiCo-LDH@$Ni(OH)_2$ heterogeneous composite as electrode material for hybrid supercapacitors, *Journal of Energy Storage*, 2023, **64**, 107213.

[7] B. Huang, W. Wang, T. Pu, J. Li, J. Zhu, C. Zhao, L. Xie and L. Chen, Two-dimensional porous (Co, Ni)-based monometallic hydroxides and bimetallic layered double hydroxides thin sheets with honeycomb-like nanostructure as positive electrode for high-performance hybrid supercapacitors, *Journal of Colloid and Interface Science*, 2018, **532**, 630-640.

[8] H.-B. Wang, H.-Y. Zeng, K. Zhang, S.-B. Lv, W. Yan, Z.-H. Tang and C.-W.

Luo, N-doped ZnCo-LDH ultrathin nanosheet array on nickel foam for high performance supercapacitors, *Journal of Alloys and Compounds*, 2024, **972**, 172701.